SPACE PROPULSION 2022, ESTORIL, PORTUGAL / 9 – 13 MAY 2022

NON STATIONARY FLUID MODELLING OF PLASMA DISCHARGE IN HALL THRUSTERS

D. Poli[1], **E. Bello-Benítez**[1], **P. Fajardo**[1], **E. Ahedo**[1]

[1]Equipo de Propulsión Espacial y Plasmas, Universidad Carlos III de Madrid, Leganés, Spain

Email: dpoli@pa.uc3m.es, ebello@ing.uc3m.es, pfajardo@ing.uc3m.es, eduardo.ahedo@uc3m.es

KEYWORDS:

Hall Thruster, Plasma modelling, 1D model

ABSTRACT

In the latest years Hall thrusters gained increasing relevance in the frame of space electric propulsion, nonetheless the physics of the plasma discharge is not yet completely understood. In this regard different models have been developed through the years trying to assess the different plasma instabilities developing within the discharge, their nonlinear evolution and saturation, and their role in yet uncharacterized phenomena such as the anomalous transport. Among the various possibilities it has been seen that fluid 1D models manage to approximate fairly well the qualitative characteristics of the plasma discharge with low complexity and computational cost. The increasing interest in characterizing axial ionization instabilities has prompted even more the community to develop new low dimensional models, which are able to capture and match experimental measurements of breathing-type oscillations. However, a common feature of these models is the oversimplification of the physics involved, which may play an important role in the overall thruster discharge dynamics. In this work, a newly developed time dependant 1D model is presented which features a more characterized heavy species dynamics, the inclusion of a downstream plume and azimuthal electrons inertia. A parametric study both on the thruster operating point and the newly introduced parameters is presented and preliminary analysis of the ionization instability has been carried out.

1 INTRODUCTION

Nowadays Hall-Effect Thrusters (HET) are commonly used devices in the frame of electric space propulsion. Nevertheless there are many aspects of the physics involved which are poorly understood or not well characterized. For instance the modeling and characterization of the cross field transport, commonly called anomalous transport, poses a relevant challenge for which no self consistent theories have been formulated yet. In order to tackle this lack of understanding, many models have been developed through the years [1], [2], utilizing different approaches such as fluid, PIC and hybrid codes.

The growing interest in understanding axial plasma oscillations in HET devices has motivated the development of time dependant 1D model both fluid [3–11] and hybrid [12], which are much less computationally expensive than 2D ones. One dimensional models allow to obtain a phenomenological characterization of the plasma discharge and due to their simplicity they can easily match experimental measurements by tuning a set of free parameters. However, due to the effects neglected by the low dimensionality, these models have not been successful in isolating the trigger mechanism of axial instabilities.

Moreover, it is common practice to oversimplify one dimensional models by employing drift-diffusion approximation (electrons inertia is neglected), using cold heavy species, neglecting neutrals dynamics and wall interactions. Even though some of these effects have a minor impact on the overall discharge, they could play an important role in the dynamical behaviour of the thruster.

While some of the oversimplifications have been removed in previous works, for example with the introduction of neutrals momentum [11] and ions energy equation [10], the presented work includes some novelties in the frame of one dimensional quasineutral models. In particular, along with the inclusion of electrons azimuthal inertia and a larger domain extending to the plume and featuring a finite thickness cathode, continuity, momentum and energy have been considered for each specie to fully characterize the dynamics of heavy particles. The effects of the added physics are evaluated through a parametric study.

The complete model is presented in Section 2, including the details on the neutrals wall interaction and the computation of the discharge current accounting for finite thickness cathode and electrons azimuthal inertia. In Section 3 the results are presented and a parametric study is performed, both on the effects of the added physics and the response of the full model to changes in the operating point. Finally a brief analysis on the observed onset of ionization instability is discussed. In this work an SPT-

100-type HET is considered as reference thruster for all the simulations.

2 MODEL FORMULATION

In this work the time dependent HET axial discharge is described with fluid equations for ions, neutrals and electrons (indexes *i, n, e*, respectively). The model is partially based on previous work from Ahedo and co-workers [4], in which the discharge is modelled as a neutral plasma with negligible pressure forces on neutrals and ions, the electrons are described using drift diffusion approximation and only the radial component of the magnetic field is considered. In more recent works [13,14], electrons azimuthal inertia and a volumetric cathode have been introduced in a stationary model. The equations reported below include some added physics such as ions and neutrals pressure terms and energy equations.

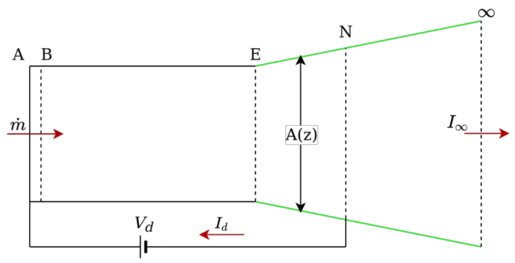

Figure 1: *The figure represents the Hall thruster model used in this work. A represents the location of the anode, B is the location of the sheath edge, which is used as boundary for the domain of the quasi-neutral model. Point E indicates the channel exit and N the centre of the volumetric cathode.*

A schematic of the computational domain is reported in Fig. 1 which includes the quasi-neutral regions of the thruster channel (*B*-*E*) and the diverging plume (*E*-∞). The point *N* indicates the location of the volumetric cathode emission centre. Outside the channel the plume divergence is accounted for as:

$$\frac{dA}{dz} = \frac{4\pi R(T_{eE}/m_i)^{1/2}}{u_{zi}} \quad \text{(Eq. 1)}$$

with T_{eE} the electrons temperature at the channel exit. The anode sheath (*A*-*B*) is supposed to be infinitely thin and it is solved analytically. The radial magnetic field magnitude is supposed to follow a Gaussian shape:

$$B(z) = B_m \exp\left[-\frac{(z-z_m)^2}{L_m^2}\right] \quad \text{(Eq. 2)}$$

where B_m is the maximum value of the magnetic field, z_m is the location of the maximum and L_m the characteristic length of magnetic decay. In general different values of L_m are used in the interior ($L_{m,in}$) and exterior ($L_{m,out}$) regions.

The model describes an axisymmetric plasma discharge by averaging the plasma properties along the radial direction. The divergence operator is thus expressed as:

$$\nabla \cdot \boldsymbol{v} = \frac{1}{A}\frac{d}{dz}(Av_z) + v' \quad \text{(Eq. 3)}$$

where $\boldsymbol{v}$ is an arbitrary vector, z the axial coordinate, A the discharge cross section and v' a term accounting for lateral wall fluxes. Being the model quasi-neutral it is assumed that $n_e = n_i$. Using standard notation, the full system of equations in their conservative form is expressed as:

$$\frac{\partial n_i}{\partial t} + \frac{1}{A}\frac{\partial (A n_i u_{zi})}{\partial z} = S_p - S_w \quad \text{(Eq. 4)}$$

$$\frac{\partial n_e}{\partial t} + \frac{1}{A}\frac{\partial (A n_e u_{ze})}{\partial z} = S_p - S_w + S_c \quad \text{(Eq. 5)}$$

$$\frac{\partial n_n}{\partial t} + \frac{1}{A}\frac{\partial (A u_{zn} n_n)}{\partial z} = -S_p + S_w \quad \text{(Eq. 6)}$$

$$\frac{\partial (n_i u_{zi})}{\partial t} + \frac{1}{A}\frac{\partial (A n_i u_{zi}^2)}{\partial z} = -\frac{1}{m_i}\frac{\partial (T_i n_i)}{\partial z} - \frac{n_i e}{m_i}\frac{\partial \phi}{\partial z} - S_w u_{zi} + S_p u_{zn} \quad \text{(Eq. 7)}$$

$$0 = -\frac{\partial (T_e n_e)}{\partial z} + n_e e\frac{\partial \phi}{\partial z} + n_e e u_{ye} B - m_e n_e u_{ze}\nu_e \quad \text{(Eq. 8)}$$

$$\frac{\partial (n_e u_{ye})}{\partial t} + \frac{1}{A}\frac{\partial (A n_e u_{ye} u_{ze})}{\partial z} = -\frac{n_e e}{m_e} u_{ze} B - n_e u_{ye}\nu_e \quad \text{(Eq. 9)}$$

$$\frac{\partial (n_n u_{zn})}{\partial t} + \frac{1}{A}\frac{\partial (A n_n u_{zn}^2)}{\partial z} = -\frac{1}{m_i}\frac{\partial (T_n n_n)}{\partial z} - S_p u_{zn} + S_w u_{znw} \quad \text{(Eq. 10)}$$

$$\frac{\partial \left(\frac{3}{2} n_i T_i\right)}{\partial t} + \frac{1}{A}\frac{\partial \left(\frac{5}{2} A n T_i u_{zi}\right)}{\partial z} = u_{zi}\frac{\partial (n_i T_i)}{\partial z} - S_w \frac{3}{2} T_i + \frac{1}{2} S_p \left(3T_n + m_i (u_{zn} - u_{zi})^2\right) \quad \text{(Eq. 11)}$$

$$\frac{\partial \left(\frac{3}{2} n_e T_e\right)}{\partial t} + \frac{1}{A}\frac{\partial \left(\frac{5}{2} A n_e T_e u_{ze}\right)}{\partial z} = -\frac{1}{A}\frac{\partial (A q_{ze})}{\partial z} + u_{ze}\frac{\partial n_e T_e}{\partial z} - S_p E_{inel} - S_w E_{ew} + m_e n_e \nu_e u_e^2 + S_c E_c \quad \text{(Eq. 12)}$$

$$\frac{\partial \left(\frac{3}{2} n_n T_n\right)}{\partial t} + \frac{1}{A}\frac{\partial \left(\frac{5}{2} A n_n T_n u_{zn}\right)}{\partial z} = u_{zn}\frac{\partial (n_n T_n)}{\partial z} - \frac{3}{2} T_n S_p + S_w \left(E_{nw} + \frac{1}{2} m_i (u_{zn}(u_{zn} - 2u_{znw}))\right) \quad \text{(Eq. 13)}$$

$$q_{ze} = -\frac{5n_eT_e}{2m_e}\frac{\nu_e}{\nu_e^2+\omega_{ce}^2}\frac{\partial T_e}{\partial z} \qquad \text{(Eq. 14)}$$

Equations (4-6) represent continuity for each specie, (7-10) the momentum and (11-13) the internal energy.

In the axial momentum of electrons (Eq. (8)) the inertial terms have been neglected, employing the drift diffusion approximation, whereas in the azimuthal electrons momentum such terms can be relevant and thus have been retained. In the above equations the source terms represent plasma production (ionization) and wall losses:

$$S_p = n_e\nu_p \qquad \text{(Eq. 15)}$$

$$S_w = n_e\nu_w \qquad \text{(Eq. 16)}$$

and expressions for the production and wall-loss frequencies are reported in the Appendix. In the above equations ν_e is the total collision frequency for electrons expressed as

$$\nu_e = \nu_t + \nu_{ei} + \nu_{en} + \nu_{wm} \qquad \text{(Eq. 17)}$$

where ν_{ei}, ν_{en} and ν_{wm} are the electron-ion, electron-neutral and momentum wall-loss frequencies, respectively. The turbulent transport ν_t is expressed as $\nu_t = \alpha_t\omega_{ce}$ with ω_{ce} the gyrofrequency (α_t can be defined for the interior and exterior region of the channel). In Eq. (12) E_{inel} is the inelastic energy loss due to ionization, S_cE_c is the energy source term accounting for the volumetric cathode, $E_{ew} = T_e$ the energy loss at the wall and q_{ze} is the axial component of the heatflux vector expressed as Eq. (14).

The term S_c in Eq. (5) represents the cathode electrons source term accounting for the volumetric cathode emission. Following the same derivation of Bello [13], the cathode source term S_c is assumed to be proportional to the discharge current and to be concentrated around the point *N* with a Gaussian distribution:

$$S_c(z) = \frac{2}{\sqrt{\pi}}\frac{I_d}{eAl_c}\exp\left[-4\frac{(z-z_N)^2}{l_c^2}\right] \qquad \text{(Eq. 18)}$$

where l_c the effective emission length and z_N the coordinate of the cathode emission centre. By subtracting the ions and electrons continuity:

$$\frac{\partial I}{\partial z} = -eAS_c(z) \qquad \text{(Eq. 19)}$$

By integrating Eq. (19) and using the definition of the cathode source term reported in Eq. (18):

$$\begin{aligned} I(z) &= I_d\hat{I}_z \\ \hat{I}_z &= \frac{1}{2}\left(1 - erf\left(2\frac{z-z_N}{l_c}\right)\right) \end{aligned} \qquad \text{(Eq. 20)}$$

where $I(z)$ is the axial profile of the discharge current, supposed to be constant in the anode cathode region and zero in the far plume. Being the model quasi neutral, in each point of the domain the axial electrons velocity is obtained from $I(z)$ and the ion current.

2.1 Neutrals Wall Interaction

A novelty of this model is the introduction of the internal energy equation for neutrals. In order to accurately model the energy sources, wall interactions must be considered. In particular it is known that ions reaching a wall might recombine with one electron (for simplicity only singly charged ions are considered) and reenter the plasma as neutrals. However, the mechanism of how this happens is seldom investigated and poorly understood, especially in the frame of HET discharges. Recent works [15] have tried to shed light on this complex phenomena by taking into account different type of wall-particle interaction models. In this model a simplified approach has been used where two accommodation parameters are employed to define the fraction of ions velocity (α_{wm}) and energy (α_{we}) that is retained by wall born neutrals. In particular the axial velocity of wall neutrals is expressed as:

$$u_{znw} = u_{zi}(1-\alpha_{wm}) \qquad \text{(Eq. 21)}$$

and their energy as:

$$E_{nw} = \left(\frac{T_e}{2} + e\Delta\phi_w + \frac{m_iu_{zi}^2}{2} + \frac{5}{2}T_i\right)(1-\alpha_{we}) \qquad \text{(Eq. 22)}$$

In the above equation the first parenthesis represents the total energy that ions deposit on lateral walls, in particular $T_e/2$ is the plasma potential with respect to the potential at the lateral sheath edge, $\Delta\phi_w$ is the sheath potential drop on lateral walls and the remaining terms are the total energy of ions before entering the pre-sheath. The sheath potential drop at the wall is computed as:

$$\Delta\phi_w = \frac{T_e}{e}\ln\left(\sqrt{\frac{m_i}{2\pi m_e}}\sigma_{rp}\left(1-\delta_s\right)\right) \qquad \text{(Eq. 23)}$$

Where σ_{rp} is the replenishment factor and δ_s is the secondary electrons emission yield. In order to account for space charge saturation of secondary electrons emission, δ_s has an upper bound such that $e\phi_w^\star/T_e^\star = \hat{\phi_w^\star}$ where the star superscript represents the saturated regime and $\hat{\phi_w^\star}$ is a constant. The saturated secondary electrons yield coefficient $\delta_s^\star$ is thus:

$$1-\delta_s^\star = \frac{3.32}{\sigma_{rp}}\sqrt{\frac{2\pi m_e}{m_i}} \qquad \text{(Eq. 24)}$$

where the constant at the numerator is computed to obtain the usual value of $\delta_s^\star = 0.983$ with $\sigma_{rp} = 1$ and $\hat{\phi_w^\star} = 1.2$ [16]. This model is a rather crude representation of the complex phenomena involving wall-particles interaction and in future works a more detailed approach might be used.

2.2 Boundary Conditions

The boundary conditions are imposed to respect the hyperbolic nature of the system, exception made for the electrons energy equation due to the diffusion term. Neutrals injection at the anode is supposed to be supersonic. The boundary conditions at the anode are:

- Neutrals injection velocity
- Neutrals injection temperature
- Neutrals injection mass flow rate accounting for ions recombination
- Electrons heatflux
- Bohm condition for ions velocity

Following [3] the anode sheath potential in the region *A-B* is expressed as:

$$\phi_{AB} = -\frac{T_{eB}}{e} \min\left(0, \ln\frac{4|u_{zeB}|}{\bar{c}_{eB}}\right) \quad \text{(Eq. 25)}$$

where $\bar{c}_{eB} = \sqrt{8T_e/\pi m_e}$ is the electrons thermal velocity. The anode electrons heatflux can thus be expressed as [17]:

$$q_{zeB} = n_B u_{zeB}\left(e\phi_{AB} - \frac{1}{2}T_{eB}\right) \quad \text{(Eq. 26)}$$

At the far plume the only imposed condition is the temperature for electrons; for all other quantities outlet conditions are used. Since the cathode is located inside the domain, the energy of injected electrons E_c, which are supposed to be injected with zero velocity, is also imposed.
In this model the discharge current is an unknown while the discharge potential is imposed between anode and cathode. In the following section a detail description of the potential boundary condition is presented.

2.2.1 Potential Boundary Condition

In drift diffusion quasi-neutral 1D models it is common [7,8,11] to derive an equation for the discharge current by integrating Eq. (8). Such equation allows to compute the current satisfying the imposed discharge potential; however, it is valid only in the anode-cathode region where the discharge current is spatially constant but can vary in time. The presented model features a larger domain extending in the plume (where the current is assumed to be zero) and it includes the effects of azimuthal electrons inertia; the current equation must be modified accordingly in order to take in account these effects. In order to account for the effects of the azimuthal inertia of electrons, Eq. (9) is written as:

$$u'_e = u_{ye} + u_{ze}\chi \quad \text{(Eq. 27)}$$

where u'_e represents the inertial effects of the azimuthal momentum equation to be evaluated at each time step. The Hall parameter is expressed as:

$$\chi = \frac{eB}{\nu_e m_e} \quad \text{(Eq. 28)}$$

Substituting Eqs. (20,27) in Eq. (8) to remove u_{ze} and u_{ye}:

$$\frac{\partial\phi}{\partial z} = \frac{1}{en_e}\frac{\partial(T_e n_e)}{\partial z} - u'_e B + \frac{u_{zi}}{\mu_{\perp e}} - \frac{I_d \hat{I}_z}{A n_e e}\frac{1}{\mu_{\perp e}} \quad \text{(Eq. 29)}$$

where the electrons perpendicular mobility as the usual expression of:

$$\mu_{\perp e} = \frac{e}{m_e \nu_e}\left(1+\chi^2\right) \quad \text{(Eq. 30)}$$

Integrating Eq. (29) and solving for I_d:

$$I_d = \frac{\int_{z_B}^{z_N}\left[\frac{1}{en_e}\frac{\partial(T_e n_i)}{\partial z} - u'_e B + \frac{u_{zi}}{\mu_{\perp e}}\right]dz + \phi_B}{\int_{z_B}^{z_N}\left[\frac{\hat{I}_z}{Aen_e}\frac{1}{\mu_{\perp e}}\right]dz} \quad \text{(Eq. 31)}$$

where $\phi_B = V_d + \phi_{AB}$ is the discharge potential plus the sheath potential at the anode computed with Eq. (25).

2.3 Solution Method

The integration of the equations is performed by writing the semi-discrete formulation using a finite volume scheme with first order Rusanov [18] fluxes for the convective terms. The diffusion term in the electrons energy equation is discretized with central differencing. The hyperbolic equations are advanced in time using an explicit second order Runge Kutta scheme where each specie is treated as a coupled system. The electrons energy equation is integrated with a semi implicit Crank-Nicolson scheme, where all the non linear terms are treated explicitly.
In order to avoid oscillations at the ions stagnation point, the electron pressure coupled method introduced by Hara [5] has been used.
In each time-step the following integration procedure is used:

1. Neutrals are advanced
2. Ions are advanced
3. All collision frequencies are update with the new density
4. Electrons energy equation is advanced
5. The new discharge current is computed
6. Electrons velocities are updated

The model is solved with an original parallel code written in Fortran. The CFL condition for electrons azimuthal momentum and ions constrains the time-step to relatively small values. A typical simulation with 2400 cells and $2\,\mathrm{ms}$ of integration time (corresponding to 10 millions iterations of the algorithm) is of roughly 20 minutes on an AMD Ryzen 5 2600X with 5 cores. Note that the computational time has room for improvements since the code has not been aggressively optimized.

3 RESULTS

The model introduced in Section 2 includes a number of effects that can have a strong impact on the solution. In order to evaluate the effects of the new equations, five configurations have been defined with increasing physics complexity:

- *Config.1*: Heavy species temperatures are constant and uniform, electrons are inertialess and neutrals have constant velocity.
- *Config.2*: Neutrals momentum equation is introduced.
- *Config.3*: Azimuthal electrons inertia is introduced.
- *Config.4*: Neutrals energy equation is introduced.
- *Config.5*: Ions energy equation is introduced.

In particular *Config.1* represents the commonly adopted model where heavy species pressure effects and neutrals dynamics are neglected. The main simulations parameters are reported in Table 1 and are kept constant for all simulations, if not explicitly specified.

Table 1: *Relevant simulation parameters for the nominal case. These parameters have been used in all the simulation if not specified.*

$\dot{m}$	$4.75\,\mathrm{mg\,s^{-1}}$	V_d	$300\,\mathrm{V}$
T_n	$0.06\,\mathrm{eV}$	$T_{e\infty}$	$1\,\mathrm{eV}$
u_{zn}	$300\,\mathrm{m\,s^{-1}}$	E_c	$5\,\mathrm{eV}$
T_i	$0\,\mathrm{eV}$	L_∞	$8.35\,\mathrm{cm}$
B_m	$250\,\mathrm{G}$	z_m	$2.5\,\mathrm{cm}$
$L_{m,in}$	$1.35\,\mathrm{cm}$	$L_{m,out}$	$1\,\mathrm{cm}$
L_E	$2.5\,\mathrm{cm}$	L_N	$3.35\,\mathrm{cm}$
A	$40\,\mathrm{cm^2}$	R	$4.25\,\mathrm{cm}$
α_t	0.0094	l_c	$0.5\,\mathrm{cm}$
α_{wm}	1	α_{we}	1

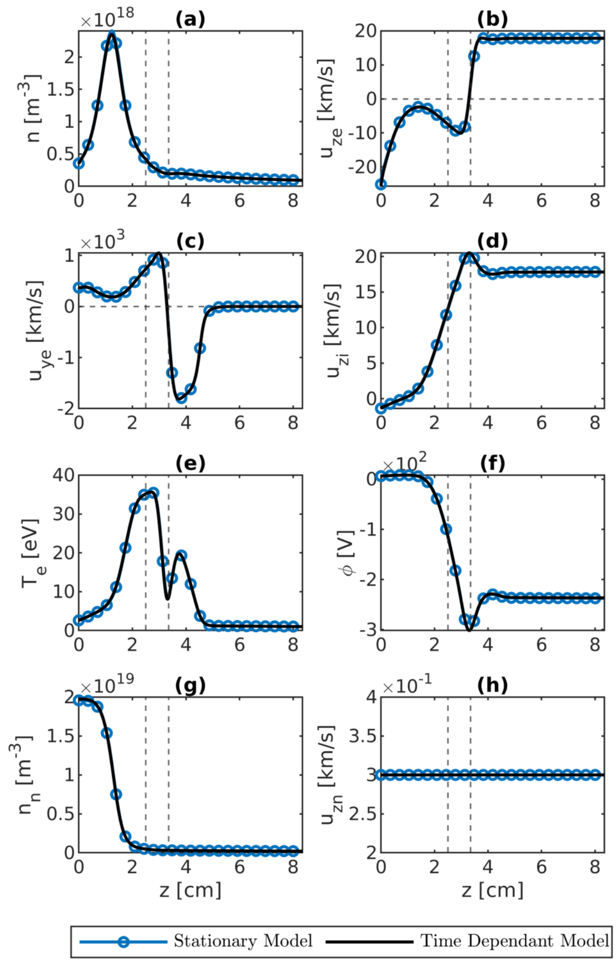

Figure 2: *Comparison of the steady state solution of the time dependant model at* $2\,\mathrm{ms}$ *with the stationary model of Bello [14]. Starting from the left the two vertical dashed lines represent the point* E *and* N *respectively. For the comparison the neutrals velocity has been considered constant.*

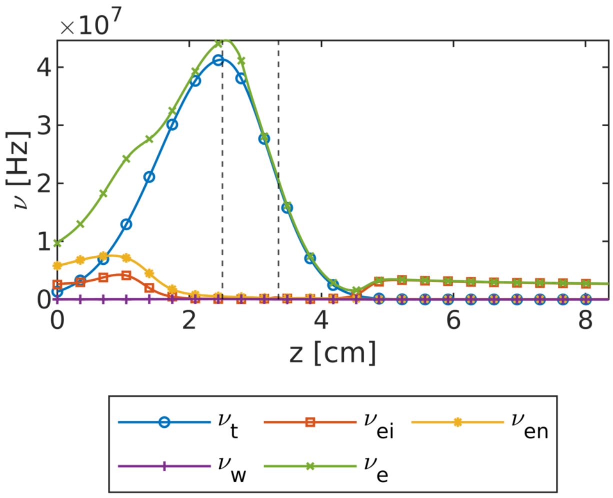

Figure 3: *Main collision frequencies for* Config.1 *at* $2\,\mathrm{ms}$. *Starting from the left the two vertical dashed lines represent the point* E *and* N *respectively.*

3.1 Stationary Model Comparison

Before performing the parametric study, the code has been validated against the stationary model developed by Bello [14]. Even though the stationary model is capable of including electrons azimuthal inertia and neutrals momentum, for the reference simulation it has been chosen to use the drift-diffusion approximation and constant neutrals velocity to better observe the effects of the added equations.
The direct comparison has been performed with the *Config.1* using the parameters reported in Table 1. It must be noted that even though the neutrals injection temperature T_n in Table 1 is larger than zero, whereas in the model by Bello heavy species are cold, this has no effect in *Config.1* being the neutrals momentum equation neglected. The steady state of the time dependant model at $2\,\mathrm{ms}$ and the stationary solution are reported in Fig. 2. As it can be seen, there is extremely good agreement between the two solutions, being the biggest difference in the plasma density maximum value. By looking at Fig. 2(a) it appears that the time dependant model slightly underestimates the plasma density with respect to the stationary one. Nevertheless the difference is negligible and it can be attributed to the numerical diffusion introduced by the solution method of the time dependant model. After the cathode, where the plasma starts to become demagnetized, the supersonic expansion of the plume results in the acceleration of the ions. The conservation of ions flux requires a decay of the plasma density, as it can be seen in Fig. 2(a). In Fig. 3 the main collision frequencies at steady state are reported.

3.2 Effects Of Added Physics

In this section the effects of including more physics in the model are evaluated. The analysis is performed by keeping all the parameters in Table 1 fixed while varying the configurations from *Config.1* to *Config.5*. The steady states of relevant discharge properties for each configuration are reported in Fig. 4. By looking at the plasma density (Fig. 4(a)) it can be observed the strong effect of neutrals momentum (*Config.2*), and thus of all the more complex configurations, in shaping the plasma discharge. From Eq. (10), noting that u_{znw} is zero due to the perfect accommodation assumption ($\alpha_{wm} = 1$), it is evident that the pressure gradient is the sole term responsible of accelerating the neutrals, being the neutrals temperature constant (in *Config.1-3*) and the neutrals density monotonically decreasing. The acceleration of neutrals results in a steeper descent of the neutrals density (Fig. 4(i)). The increased electrons temperature in the channel (Fig. 4(e)) and the steeper neutrals density profile contribute in shifting the ionization (Fig. 4(k)) and plasma density peaks towards the anode. It is interesting to note that the resulting ionization frequency is larger; the lower plasma density can than be explained by looking at the zoomed detail in Fig. 4(d) where a larger ions velocity can be observed. The effects of azimuthal inertia can be apreciated in the profiles downstream the cathode of u_{ye} (see Fig. 4(c)) and of T_e (see Fig. 4(c)).

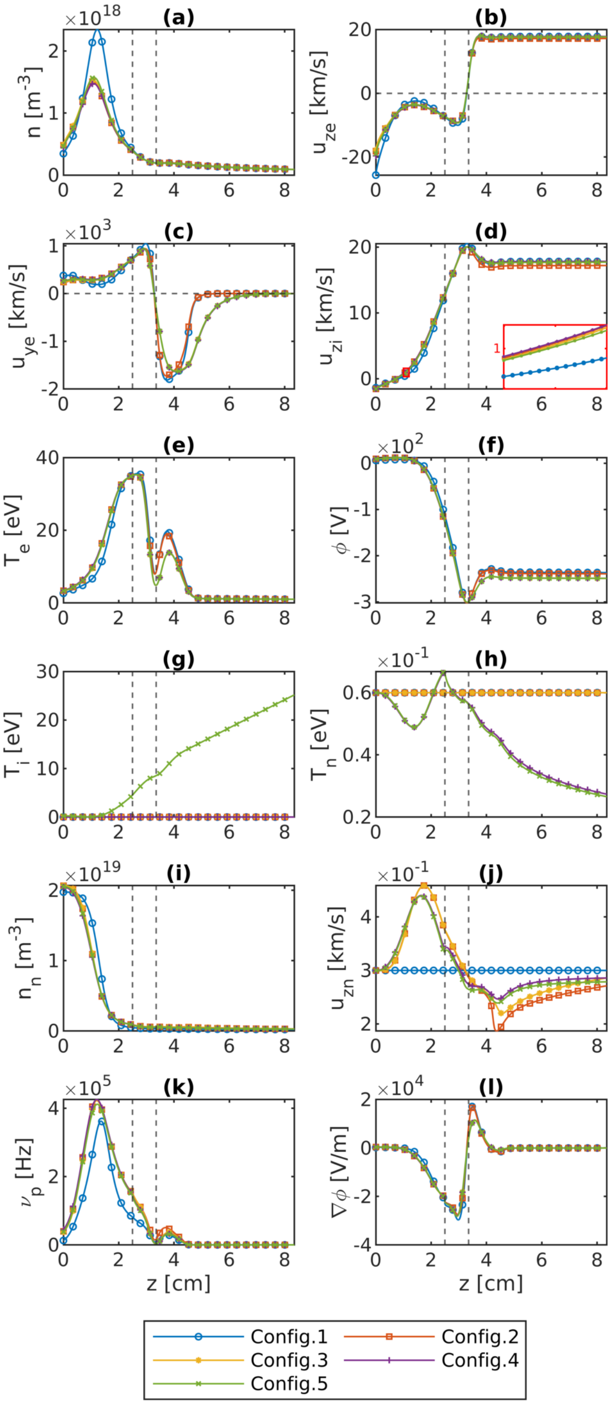

Figure 4: *Steady state for different configurations of the time dependant model. Perfect accommodation for neutrals wall interactions is considered. Starting from the left the two vertical dashed lines represent the point* E *and* N *respectively.*

The lower absolute value of the azimuthal velocity, in the case with inertia, is responsible of a lower collisional heating and thus a lower electrons temperature. In accordance with the findings from Bello [13], the azimuthal velocity decays differently in the unmagnetized region of the discharge where it is the inertia instead of the magnetic force that counteracts the collisional force. Finally, due to the perfect accommodation assumption ($\alpha_{wm} = 1$ and $\alpha_{we} = 1$), neutrals are mostly cooled by ionization being wall sources neglected whereas ions are heated. The large ions temperature in the plume can be explained by looking at the term $(u_{zn} - u_{zi})^2$ in Eq. (11), being the ions downstream velocity almost two orders of magnitude larger than the neutrals one.

3.3 Performance Analysis

In this section the effects of operational parameters on the stationary discharge are analysed. In particular injected mass flow rate, discharge potential and internal magnetic field decay are considered. Some of the relevant performance parameters are taken in to account such as the thrust F, the discharge current I_d, the utilization efficiency η_u, the current efficiency η_c, the energy efficiency η_e and the thrust efficiency η, expressed respectively as:

$$F = m_i \sum_{s=i,n} \left[\left(n_s u_{zs}^2 A \right) + n_e T_e A \right]_\infty \qquad \text{(Eq. 32)}$$

$$\eta_u = \frac{m_{i\infty}}{\dot{m}} \qquad \text{(Eq. 33)}$$

$$\eta_c = \frac{I_{i\infty}}{I_d} \qquad \text{(Eq. 34)}$$

$$\eta_e = \frac{F^2}{2\dot{m}_{i\infty} I_{i\infty} V_d} \qquad \text{(Eq. 35)}$$

$$\eta = \frac{F^2}{2 I_d V_d \dot{m}} = \eta_u \eta_c \eta_e \qquad \text{(Eq. 36)}$$

where the subscript ∞ stands for the far plume and $I_{i\infty}$ and $\dot{m}_{i\infty}$ are the downstream ion current and mass flow rate.
The operational parameters are varied once at a time keeping all the other parameters as the ones in Table 1.

3.3.1 Effects Of Mass Flow Rate

The first parameter analysed is the injected mass flow rate, which is the amount of propellant (Xenon in this case) that each second is fed to the thruster during its operation. In Table 2 the relevant performance parameters are reported for each of the simulated cases.

Table 2: *Performance parameters for different values of the injected mass flow rate. The other parameters are kept constant for each simulation.*

$\dot{m}$	F	I_d	η_u	η_c	η_e	η
[mg/s]	[mN]	[A]	[%]	[%]	[%]	[%]
4.25	70.1	4.50	94.0	65.1	70.1	42.8
4.75	80.4	5.16	95.4	64.4	71.6	44
5.25	90.5	5.81	96.4	63.9	72.7	44.8
5.75	100.4	6.45	97.1	63.5	73.5	45.3

It can be observed that both the thrust and the efficiency increase with larger injected mass flow rates. On the contrary the current efficiency becomes lower, meaning that a larger fraction of the discharge current is spent in sustaining the plasma discharge.

3.3.2 Effects Of Discharge Potential

The discharge potential is one of the main parameters of an HET discharge since it is the potential difference, sustained thanks to the reduced axial electrons mobility, that eventually accelerates the ions to generate thrust. The performance parameters at different operating point are reported in Table 3.

Table 3: *Performance parameters for different values of the discharge potential. The other parameters are kept constant for each simulation.*

V_d	F	I_d	η_u	η_c	η_e	η
[V]	[mN]	[A]	[%]	[%]	[%]	[%]
255	72.2	4.93	95	67.1	68.4	43.6
275	76	5.04	95.2	65.8	70	43.9
300	80.4	5.16	95.4	64.4	71.6	44
350	88.4	5.37	95.5	62	73.9	43.8
475	106.5	5.83	96.1	57.5	78	43.1
525	113.2	6	96.4	55.9	79.4	42.8
625	125.9	6.32	96.9	53.4	81.6	42.2

All the simulations present a steady state, exception made for the last case at $625\,\mathrm{V}$ for which high frequency oscillations appear. The oscillation frequency is in the 350-$400\,\mathrm{kHz}$ range, which is compatible with the Ion Transit Mode (ITT) [19]. From Table 3 it is interesting to note that the efficiency presents a maximum for the case at $300\,\mathrm{V}$.

3.3.3 Effects of Internal Magnetic Field Decay

As briefly discussed in Section 2 in the radial magnetic field model adopted (Eq. (2)), the L_{mi} parameter is responsible for the shape of the magnetic field in the channel region. In practice the profile of the magnetic field decay is important for the discharge since it is responsible for the reduced axial electrons mobility due to the establishment of the azimuthal current. The magnetic field at the anode assumes

the values reported in the second column of Table 4. The magnitude of the radial magnetic field in the near anode region is important since it influences directly the ratio of the ion current at the anode over the total discharge current, as it can be seen in Table 4. The anode ion current, or ion back-flow, is essential for having a sustained plasma discharge. It has been seen that for some parameters, usually during the onset of ionization instabilities, the ion-discharge current ratio becomes very small and eventually the back-flow region is extinguished leading to a failure of the code.
The performances for different values of the magnetic field decay characteristic length are reported in Table 4.

Table 4: *Performance parameters for different values of the internal magnetic field decay. The magnetic field at the anode in Gauss and the ratio between the ion current at the anode and the total discharge current are reported in the second and third column, respectively.*

L_{mi}	B_A	$\lvert I_{iA}\rvert/I_d$	F	I_d	η
[cm]	[G]	[%]	[mN]	[A]	[%]
1.25	4.60	11.41	80	5.21	43.1
1.30	6.22	10.16	80.3	5.19	43.6
1.35	8.14	8.89	80.4	5.16	44
1.40	10.35	7.61	80.6	5.13	44.3

As it can be seen by increasing the characteristic length of decay, which results in a larger anode magnetic field, the thruster efficiency increases. This is to be expected since a larger magnetic field means more confined electrons (or smaller cross field transport) resulting in a smaller discharge current for the same discharge potential. Since the thrust is not negatively affected, but instead it increases slightly, from Eq. (36) it is readily seen that the efficiency must increase.

3.4 Effects Of Neutrals Wall Interactions

As already discussed in Section 2.1, heavy particles wall interaction is a very complex phenomena seldomly studied in the frame of Hall thrusters. A detailed modelling of such interactions is out of the scope of this work, which is limited to a phenomenological characterization based on two free parameters. Plasma discharge parameters are reported in Fig. 5 for different values of the wall energy accommodation factor.
For the cases corresponding to $(1-\alpha_{we}) = 1$ to 2%, mean values have been used due to the presence of breathing or not completely damped oscillations in the latter ones (inside the integration time of $2\,\mathrm{ms}$).
Extremely evident are the effects of the increased neutrals energy input on neutrals temperature, velocity and ions temperature (see Fig. 5 (h), (j), (g)). By looking at Eq. (11) there is no direct influence of the wall energy coefficient, but its effect are accounted for in the energy sources due to neutrals ionization; in particular the term $(u_{zn} - u_{zi})^2$ is responsible for mitigating the ions temperature in the plume due to a smaller velocity difference between the heavy species. Nevertheless these effects are important mostly in the plume, which is of minor interest for the dynamics of the HET discharge. Inside the channel it is possible to appreciate plasma density, ionization and electrons temperature variations; in particular higher mean plasma density is observed for higher energy inputs to neutrals (lower α_{we}) which analogously as in Section 3.2 is associated to a lower ions velocity inside the channel (see Fig. 5(d)).
In Table 5 performance parameters for each of the analysed case are reported.

Table 5: *Performance parameters for different values of the wall energy accommodation factor for neutrals.*

$1-\alpha_{we}$	F	I_d	$\lvert I_{iA}\rvert/I_d$	η
[%]	[mN]	[A]	[%]	[%]
0	80.4	5.16	8.89	44
0.5	81.9	5.22	8.56	45
1	82.7	5.29	6.35	45.6
1.5	83.2	5.30	5.21	45.9
2	82.9	5.26	4.1	46

As previously mentioned in Section 3.3.3 the anode current over total discharge current ratio can be important for the numerical solution of the code. In Table 5 it can be seen how reducing the wall accommodation parameter leads to a reduction of the anode current ratio. This trend can be observed also in Fig. 5(b) where to lower accommodation parameters correspond larger absolute values of the electrons velocity (and thus current) at the anode. In particular the $(1-\alpha_{we}) = 2\%$ case presents an average value of 4.1%, which is still adequate, but it reaches values as low as 1.9% during breathing mode oscillations. For what concern the neutrals wall momentum accommodation parameter, α_{wm}, the impact on the plasma discharge is much less relevant, as it can be seen in Fig. 6 where the steady state solutions for different values of α_{wm} are reported. In particular it seems that the wall momentum accommodation parameter has a negligible effect on the plasma parameters inside the channel. Such behaviour can be explained by observing that the ions velocity in the first part of the channel is small and thus u_{znw} will be small as well. In the plume the ions velocity is much higher but the very high accommodation factor results again in a small increment of velocity. Lower values of accommodation factor cannot be used due to the excessive cool down of neutrals, as it can be seen in Fig. 6(h), being the energy of wall born neutrals E_{wn} in Eq. (13) neglected for the assumption of $\alpha_{we} = 1$.

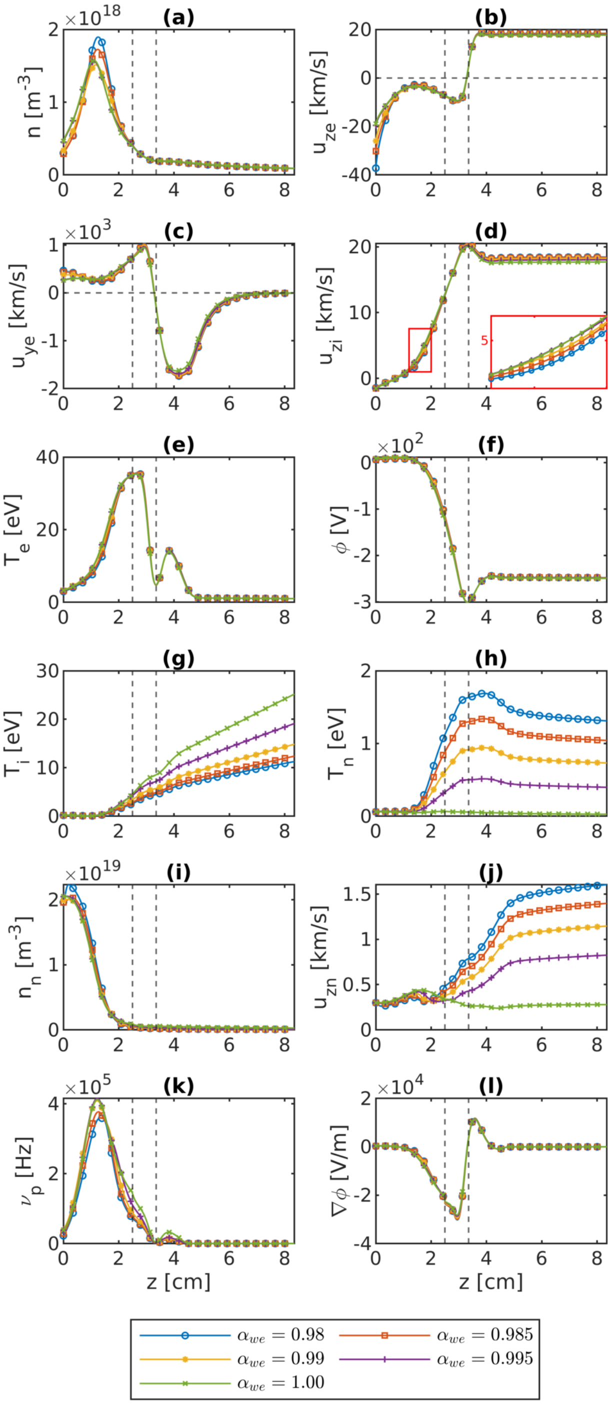

Figure 5: *Plasma discharge parameters for* Config.5 *at different* α_{we}*. For the cases* $(1 - \alpha_{we}) = 1$ *to* 2% *mean values have been considered due to the presence of breathing mode or not completely damped oscillations. Starting from the left the two vertical dashed lines represent the point* E *and* N *respectively.*

In general, a more realistic approach would be to set both parameters different from unity. However, it is expected for ions to loose the majority of their energy in the recombination process, which means that α_{we} and α_{wm} must be close to one. If that is the case, as it can be seen in Fig. 5 and Fig. 6, the effects of the wall momentum parameter are of much smaller entity with respect to the wall energy parameter. For this reason in the following sections perfect accommodation for the wall momentum has been considered.

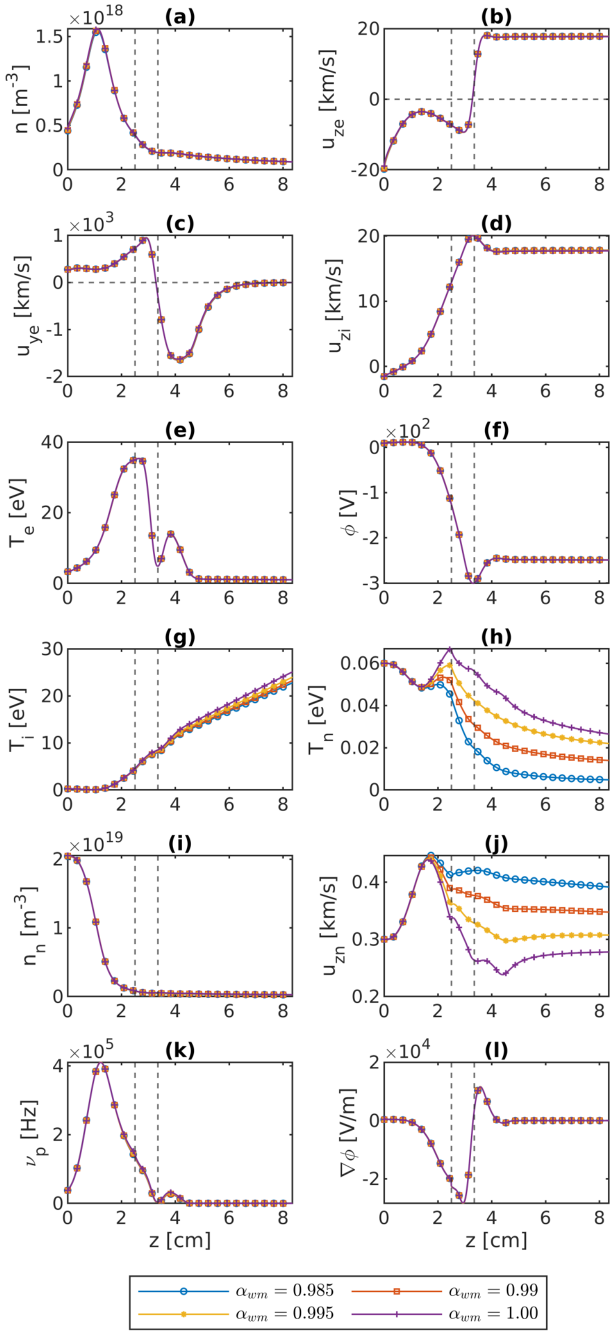

Figure 6: *Plasma discharge parameters for* Config.5 *at different* α_{wm}*. Starting from the left the two vertical dashed lines represent the point* E *and* N *respectively.*

3.5 Ionization Instability

Even though a detailed analysis of the ionization instability, commonly called breathing mode, is out of the scope of this work, in this section a brief description of the observed behaviours is reported.

If perfect accommodation is considered, $\alpha_{we} = 1$, $\alpha_{wm} = 1$, all the cases analysed at different operating point (variation of L_{mi}, V_d, $\dot{m}$) present non oscillatory solution, exception made for the case at $625\,\mathrm{V}$ which does not present breathing mode, but instead oscillate at much higher frequency.
However, as already mentioned in Section 3.4, if the neutrals wall energy parameter is decreased, allowing for more ions energy to be retained by wall born neutrals, the onset of ionization instability is observed. In particular such behaviour is experienced for $\alpha_{we} = 0.98$ whereas all the other parameters are the same as in Table 1. For smaller values of the wall energy parameter the oscillations increase in amplitude, the anode ion current fraction becomes smaller and eventually the ions backflow region is extinguished, leading to the failure of the simulation. In the following sections a brief analysis of the ionization instability is presented, taking as reference condition the one with $\alpha_{we} = 0.98$.

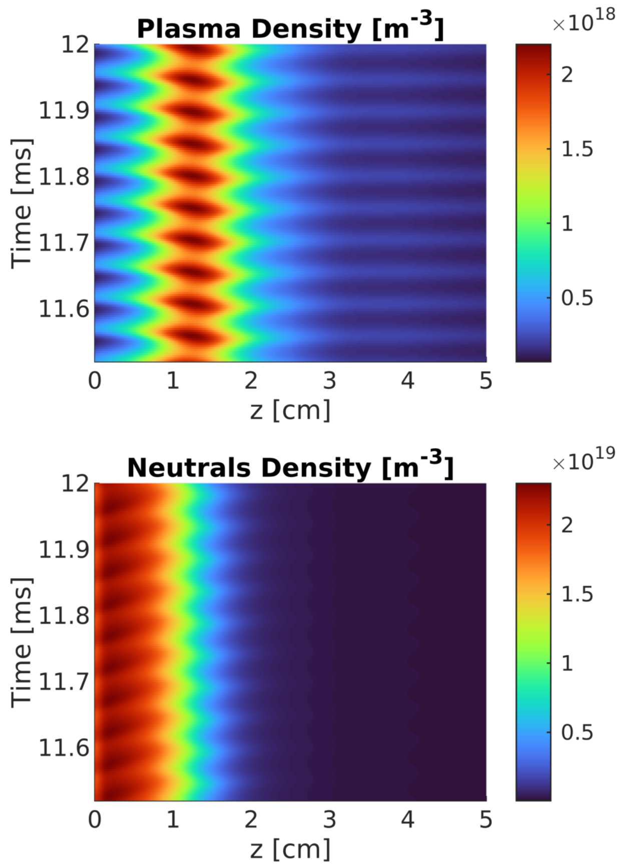

Figure 7: *Stable breathing mode obtained with* Config.5 *where* $\alpha_{we} = 0.98$ *and the other parameters as in Table 1. The integration time has been extended up to* $12\,\mathrm{ms}$*. The brathing mode oscillation frequency is of* $20.5\,\mathrm{kHz}$*.*

3.5.1 Added Physics

As observed in [10,11], in general the introduction of the neutrals momentum equation in 1D fluid models leads to stationary solutions, and thus the breathing mode is dampened. The presented model exhibits the same behaviour where damped solutions are found for the configurations *1-4*. However for *Config.5*, corresponding to the inclusion of all the equations, stable breathing mode is observed, as reported in Fig. 7. Even though a detailed theory is yet to be formulated, it seems that both neutrals wall interactions and a more detailed physical description for the heavy species play a role in obtaining stationary oscillations.

3.5.2 Replenishment Factor

In Section 2.1 the lateral wall sheath potential has been introduced to compute the energy deposited by ions reaching the channel walls. In this work it has been assumed that the $e\phi_w/T_e$ ratio for the space charge saturated regime, which corresponds to the condition where that ratio is minimum, is constant. This means that by changing the replenishment factor σ_{rp} the saturated secondary electron emission yield must change accordingly, following Eq. (24). In recent works it has been seen how the replenishment factor is linked, among other parameters, to the angle between the magnetic field and the wall [20](the default condition for this model is a perpendicular magnetic field). In Table 6 the results on breathing mode parameters are reported for different σ_{rp}.

Table 6: *Breathing mode parameters for different values of the replenishment factor* σ_{rp}*. In the last column the value of the maximum electrons temperature is reported.*

σ_{rp}	$\delta_s^\star$	f	ΔI_d	I_d	$\max T_e$
[-]	[-]	[kHz]	[A]	[A]	[eV]
1.00	0.983	20.5	2.15	5.26	35.7
0.9	0.981	20.5	2.07	5.27	36.2
0.8	0.979	20.5	1.95	5.28	37
0.7	0.976	21	1.76	5.29	38.3
0.6	0.971	21	1.60	5.31	40
0.5	0.966	21	1.74	5.31	42.1
0.4	0.957	21	2.5	5.32	44.9

As it can be seen from the table, breathing mode frequency and mean discharge current are not greatly affected by changes in the replenishment factor and saturated secondary electrons emission yield, whereas the oscillation amplitude varies of more than 50% and presents a minimum corresponding to $\sigma_{rp} = 0.6$. However, when the lateral wall plasma sheath is in a space charge saturated regime, electrons energy wall losses depend on $\delta_s^\star$. In the last column of the table the time averaged maximum value of the electrons temperature is reported, which as expected increases with lower $\delta_s^\star$ due to lower wall losses. A more realistic approach would be to take into account also the variation of the radial plasma density average coefficient $\tilde{\nu}_w$ (see Appendix), which is strongly dependant on the magnetic field distribution. A better characterization of such parameter is reserved for future studies.

4 CONCLUSIONS

In this article a newly developed 1D time dependant quasi-neutral model for HET discharges is presented. While previous models tend to neglect heavy species dynamics, in the presented work ions and neutrals energy equations, along with neutrals momentum, have been introduced. Moreover the presented model enables the possibility of extending the simulation domain to the far plume, featuring a finite thickness cathode, and of evaluating electron inertia effects by retaining the azimuthal inertia terms in the electrons momentum equation. The effects of plasma wall interaction has been introduced in neutrals dynamics by accounting for recombined ions. The rather simple model that has been adopted consists of two accommodation parameters for the wall born neutrals velocity and energy, expressed as fractions of the ions ones.

The model response to variations of the operating point has been tested by performing a parametric study on the propellant mass flow rate, discharge potential and magnetic field shape. The effects of wall born neutrals energy and velocity have been investigated, showing a limited influence of wall neutrals velocity on the discharge properties. A more substantial impact on the Hall discharge has been observed when varying the energy of wall neutrals, affecting both plasma and neutrals dynamics.

Finally a brief study on the onset of the ionization instability is presented. Even though no theory has been formulated, it has been observed that a more detailed heavy species physical description can be important for the onset of stable breathing mode. In particular as soon as the neutrals momentum equation is introduced, no stable oscillations are obtained unless the full model is considered and the neutrals receive a sufficiently high energy input.

This work has pointed out the relevance of heavy species dynamics, with particular attention to neutrals which are commonly neglected in 1D time dependant models. The introduction of azimuthal inertia and a finite thickness cathode enable the future investigation of high frequency dynamics and of the plume region.

ACKNOWLEDGMENTS

This research has been carried out in the frame of the projects SIMTURB-CM, founded by Comunidad de Madrid, and ESPEOS, funded by Agencia Estatal de Investigación with grant number PID2019-108034RB-I00.

Appendix A COLLISION FREQUENCIES

This appendix contains the expressions for the collision frequencies used in equations 4-13 and the values for the constants used in this work. The expressions here reported comes from previous work of Ahedo and co-workers [3, 4, 17].
The ionization (or production) frequency ν_p is expressed as $\nu_p = n_n \bar{c}_e \bar{\sigma}_{ion}$ where:

$$\bar{\sigma}_{ion} = \sigma_{ion,0}\left[1 + \frac{T_e E_{ion}}{(T_e + E_{ion})^2}\right]\exp\left(-\frac{E_{ion}}{T_e}\right) \quad \text{(Eq. 37)}$$

and E_{ion} is the first ionization energy. For Xenon $E_{ion} = 12.1\,\mathrm{eV}$, $\sigma_{ion,0} = 5\times10^{-20}\,\mathrm{m}^2$. The effective energy loss due to ionization, E_{inel}, satisfies:

$$E_{inel} = E_{ion}\left(2 + \frac{1}{4}\exp\left(\frac{2E_{ion}}{3T_e}\right)\right) \quad \text{(Eq. 38)}$$

The elastic electron-neutral collision frequency is $\nu_{en} = n_n \bar{c}_e \sigma_{en}$ where the cross section for Xenon is taken constant and equal to $\sigma_{en} = 27\times10^{-20}\mathrm{m}^2$. The electron-ion collision frequency is $\nu_{ei} = n_i R_{ei}$, where R_{ei} is expressed as:

$$\frac{R_{ei}}{10^{-12}m^3s^{-1}} = 2.9\cdot\left(\frac{1eV}{T_e}\right)^{3/2}\ln\Lambda \quad \text{(Eq. 39)}$$

and the Coulomb logarithm:

$$\ln\Lambda \approx 9 + \frac{1}{2}\ln\left[\left(\frac{10^{18}m^{-3}}{n_e}\right)\left(\frac{T_e}{1eV}\right)^3\right] \quad \text{(Eq. 40)}$$

The wall loss frequency is computed as:

$$\nu_w = \tilde{\nu}_w \frac{2\pi R}{A_c} c_s \quad \text{(Eq. 41)}$$

with $\tilde{\nu}_w$ a constant accounting for the radial average of the plasma density, which decreases near the wall. In this work $\tilde{\nu}_w = 0.17$. The wall loss frequency for energy and momentum are respectively $\nu_{we} = \beta_e \nu_w$ and $\nu_{wm} = \beta_m \nu_w$ with:

$$\beta_e = 5.62 + \frac{1.65}{1-\delta_s} \quad , \quad \beta_m = \frac{\delta_s}{1-\delta_s} \quad \text{(Eq. 42)}$$

Here, δ_w is the effective secondary electron emission yield from the wall, modeled as

$$\delta_s = \begin{cases} \sqrt{T_e/T_1} & \text{if } T_e < T_e^\star \\ \delta_s^\star & \text{if } T_e \geq T_e^\star = T_1 \delta_s^{\star 2} \end{cases} \quad \text{(Eq. 43)}$$

where T_1 is the temperature theoretically leading to a 100% yield (material dependant), and $T_e^\star$ is the temperature at which space charge saturation is reached. In this work $T_1 = 36.77\,\mathrm{eV}$ and $\delta_s^\star$ is computed to obtain the imposed saturated wall sheath potential, as discussed in Section 2.1.

REFERENCES

[1] Taccogna, F. and Garrigues, L., "Latest progress in Hall thrusters plasma modelling," *Reviews of Modern Plasma Physics*, Vol. 3, No. 1, 2019, pp. 12.

[2] Boeuf, J., "Tutorial: Physics and modeling of Hall thrusters," *J. Applied Physics*, Vol. 121, No. 1, 2017, pp. 011101.

[3] Ahedo, E., Martínez-Cerezo, P., and Martínez-Sánchez, M., "One-dimensional model of the plasma flow in a Hall thruster," *Physics of Plasmas*, Vol. 8, 2001, pp. 3058–3068.

[4] Ahedo, E., Gallardo, J., and Martínez-Sánchez, M., "Effects of the radial-plasma wall interaction on the axial Hall thruster discharge," *Physics of Plasmas*, Vol. 10, No. 8, 2003, pp. 3397–3409.

[5] Hara, K., "Non-oscillatory quasineutral fluid model of cross-field discharge plasmas," *Physics of Plasmas*, Vol. 25, No. 12, 2018, pp. 123508.

[6] Sahu, R., Mansour, A., and Hara, K., "Full fluid moment model for low temperature magnetized plasmas," *Physics of Plasmas*, Vol. 27, No. 11, 2020, pp. 113505.

[7] Giannetti, V., Saravia, M. M., Leporini, L., Camarri, S., and Andreussi, T., "Numerical and Experimental Investigation of Longitudinal Oscillations in Hall Thrusters," *Aerospace*, Vol. 8, 05 2021, pp. 148.

[8] Barral, S. and Ahedo, E., "Low-frequency model of breathing oscillations in Hall discharges," *Physical Review E*, Vol. 79, 2009, pp. 046401.

[9] Barral, S., Makowski, K., Peradzynski, Z., Gascon, N., and Dudeck, M., "Wall material effects in stationary plasma thrusters. II. Near-wall and in-wall conductivity," *Phys. Plasmas*, Vol. 10, No. 10, 2003, pp. 4137–4152.

[10] Hara, K. and Mikellides, I. G., *Characterization of low frequency ionization oscillations in Hall thrusters using a one-dimensional fluid model*.

[11] Chapurin, O., Smolyakov, A., Hagelaan, G., Boeuf, J., and Raitses, Y., "Fluid and hybrid simulations of the ionization instabilities in Hall thruster," 36^{th} *International Electric Propulsion Conference*, No. IEPC-2019-762, Electric Rocket Propulsion Society, Fairview Park, OH, Vienna, Austria, 2019.

[12] Hara, K., Boyd, I. D., and Kolobov, V. I., "One-dimensional hybrid-direct kinetic simulation of the discharge plasma in a Hall thruster," *Physics of Plasmas*, Vol. 19, No. 11, 2012, pp. 113508.

[13] Bello-Benítez, E. and Ahedo, E., "Advances on low-dimensionality fluid modelling of Hall thruster discharges," *Space Propulsion Conference 2021*, No. 00133, Association Aéronautique et Astronautique de France, March 17-19, 2021.

[14] Bello-Benítez, E. and Ahedo, E., "Axial-azimuthal, high-frequency modes from global linear-stability model of a Hall thruster," *Plasma Sources Science and Technology*, Vol. 30, No. 3, mar 2021, pp. 035003.

[15] Domínguez-Vázquez, A., Cichocki, F., Merino, M., Fajardo, P., and Ahedo, E., "On heavy particle-wall interaction in axisymmetric plasma discharges," *Plasma Sources Science and Technology*, Vol. 30, No. 8, aug 2021, pp. 085004.

[16] Hobbs, G. and Wesson, J., "Heat flow through a Langmuir sheath in the presence of electron emission," *Plasma Physics*, Vol. 9, 1967, pp. 85.

[17] Ahedo, E., Gallardo, J., and Martínez-Sánchez, M., "Model of the plasma discharge in a Hall thruster with heat conduction," *Physics of Plasmas*, Vol. 9, No. 9, 2002, pp. 4061–4070.

[18] Rusanov, V., "The calculation of the interaction of non-stationary shock waves and obstacles," *USSR Computational Mathematics and Mathematical Physics*, Vol. 1, No. 2, 1962, pp. 304–320.

[19] Choueiri, E., "Plasma oscillations in Hall thrusters," *Physics of Plasmas*, Vol. 8, No. 4, 2001, pp. 1411–1426.

[20] Marín-Cebrián, A., Domínguez-Vázquez, A., Fajardo, P., and Ahedo, E., "Macroscopic plasma analysis from 1D-radial kinetic results of a Hall thruster discharge," *Plasma Sources Science and Technology*, Vol. 30, No. 11, November 2021, pp. 115011.